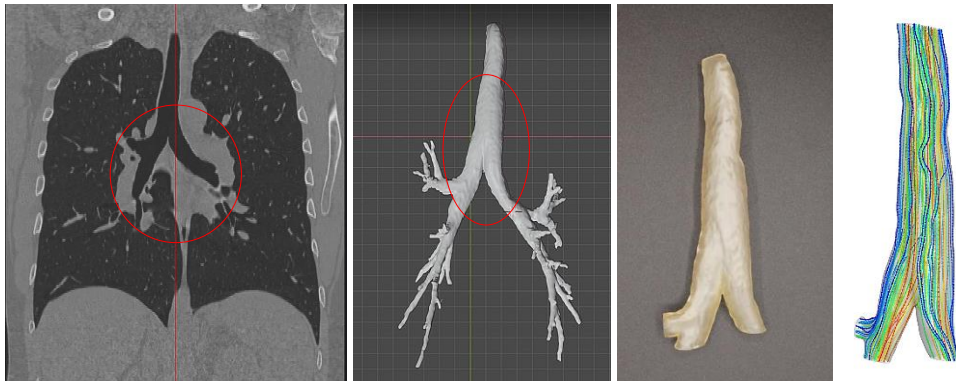




## MUCCA – Multi-disciplinary Use Case for Convergent new Approaches to AI explainability

Report II – **Experimental and numerical investigations  
of air-ways flows in the presence of mucus**  
part I – 2021



Partner 5 – University Politehnica of Bucharest, RO  
REOROM Laboratory; PI – Prof. Corneliu Balan

## PREAMBLE

From the perspective of the REOROM group, partner 5 in the MUCCA project, the central subject of the research is the investigation of the air flow in the vicinity of walls (i.e. *trachea*) in the presence of deformable viscoelastic materials (i.e. *mucus*). The goal of the study is to understand, to model and to quantify the interaction between air and the viscoelastic fluids in a confined geometry, in particular to determine the influence of the mucus on the air flow rate distribution in trachea bifurcation. The difficulty of the problem is mainly given by four factors:

(i) the flow domain (i.e. trachea's first bifurcation) has a complex geometry; the procedure to transform an CT image/picture of the bifurcation in a real physical domain is not simple,

(ii) the viscoelastic material used *in vitro* experiments is a complex fluid (similar rheology with the mucus); its modeling and rheological characterizations need tests in shear and extensional flows,

(iii) numerical simulations take long time to produce valid data; the correlation with experiments is not trivial,

(iv) the design of a procedure to analyze the results with the target to transform it in an algorithm compatible with AI and ML applications has a high degree of novelty for us.

*In this context, we create a project framework where the research activities take place. One goal is to investigate the interaction: complex fluid – air flow, and to model the dynamics of a fluid interface following a compatible procedure with a Deep Learning (DL) algorithm, respectively. We call our approach as a **Learning Deep (LD)** procedure. In the present study we intend to apply LD procedure to the modeling of mucus – air interface in the vicinity of trachea's first bifurcation.*

Dynamics of the fluid interfaces (liquid-liquid or liquid-gas) is one of the fundamental topics of study in applied physics and fluid mechanics, with relevance in almost all scientific areas, with great impact in developing novel technologies directly related to our daily life. Instabilities and breakup/rupture of the fluid interface are in the center of the investigations in relation to many applications: (i) control of the interfaces, (ii) evolution of complex interfaces between viscoelastic fluids, (iii) dynamics of the interfaces in micro-geometries and corresponding numerical simulations, (iv) novel applications in laser-physics, (v) porous media, (vi) experimental devices, visualizations techniques and image processing. In present, the fundamental research in the area is mainly focused to the study of the interface's stability, the break-up mechanism and drop formation in confined configurations, fragmentation mechanism of liquid sheets and droplets generation.

Despite a lot of published papers, many applications and novel technologies developed in various domains (engineering, medicine, biology ...), is still missing a general macro-scale model to represent the dynamics of fluid-liquid interface, to understand the influence of the rheology on the phenomenon and to model the evolution of interface in the vicinity of solid surfaces. However, the starting points of all studies are: (i) the theory behind the interface's representation and (ii) the visualizations of the interface.

The present approach is somehow similar to an inverse problem in fluid mechanics: instead to find a solution of a well-posed problem (with proper input data and given boundary/initial conditions), the aim is to determine the flow domain which generates the solution; the output is given, and we look for the input! Instead to determine the flow rate distribution in a bifurcation with a given liquid rheology inside, we try to determine the liquid's properties by processing the image of the deformable fluid interface in the investigated confined geometry. Instead to use an existing DL-algorithm to find a solution in the flow domain, we are learning deep the fundamental of the flow modelling and ML-procedures to obtain at the end a DL-algorithm to establish the mucus properties for a given deformable flow domain and air dynamics inside the trachea. So, if the flow rate distribution in the tracheal bifurcation is measured and the deformation of the internal flow configuration due to mucus transport within trachea is recorded, there is expected to determine *in vivo* the mucus rheological properties. Of course, the target is very ambitious and difficult to be reached but, applying this procedure, there are fair chances to relate the mucus rheology to the air distribution in the trachea's bifurcation, and finally to the mucus composition (and implicitly to some lung dysfunctions).

In conclusion, we are looking to establish a procedure to find the relation between the interface breakup/dynamics and the rheological properties of the fluids in a confined geometry. The project explores the possibility to apply ML-algorithms (initially developed for turbulence<sup>1</sup>), to the modelling of the viscoelastic fluid interface<sup>2</sup>; there is proposed a method to correlate the images of interfaces with the

<sup>1</sup> Kutz J.N. (2017) *Deep learning in fluid mechanics*, JFM 814, 1-4; Brunton S.L., Noack B.R., Koumoutsakos P. (2020) *Machine learning for fluid mechanics*, Annu. Rev. Fluid Mech. 52, 477-508; Kochkov D. Smith J.A., Alieva A., Wang Q., Brenner M.P, Hoyer S. (2021) *Machine learning – accelerated computational fluid dynamics*, PNAS 118(21) 2101784118; Berkooz G., Holmes Ph., Lumley J.L. (1993) *The proper orthogonal decomposition in the analysis of turbulent flows*, Annu. Rev. Fluid Mech. 25. 539-575; Lusch B., Kutz J.N., Brunton S.L. (2018) *Deep learning for universal linear embeddings of non-linear dynamics*, Nat. Comm., 9:4950; Brunton S.L., Hemati M.S., Taira K. (2020) *Special issue on machine learning and data-driven methods in fluid mechanics*, Theor. Comput. Fluid Dyn. 34, 333-337

<sup>2</sup> Buhendwa A., Adami S., Adams N. (2021) *Inferring incompressible two-phase flow from the interface motion using physics-informed neural networks*, Machine Learning and Applications 4, 100029; Gibou F., Hyde D., Fedkiw R. (2019) *Sharp interface approaches and deep learning technique for multiphase flows*, J. Comp. Physics. 380, 442-463

rheological data using an algorithm, which is expected to be extended in the framework of DNN applications (1).

“Artificial intelligence (AI) is the broadest term used to classify machines that mimic human intelligence. It is used to predict, automate, and optimize tasks that humans have historically done, such as speech and facial recognition, decision making, and translation. Machine learning (ML) is a subfield of artificial intelligence. Deep learning (DL) is a subfield of machine learning, and neural networks make up the backbone of deep learning algorithms. These neural networks (DNN) attempt to simulate the behavior of the human brain – albeit far from matching its ability – allowing it to “learn” from large amounts of data. The “deep” in deep learning is referring to the depth of layers in a neural network (2). While a neural network with a single layer can still make approximate predictions, additional hidden layers (3) can help to optimize and refine for accuracy. A neural network that consists of more than three layers, which would be inclusive of the inputs and the output, can be considered a deep learning algorithm.”<sup>3</sup> In image processing, the Deep Learning algorithms can determine which parts of the image are the most important for the application by themselves. In Machine Learning, this hierarchy of features is established manually by a human expert<sup>4</sup>. “In AI and ML there are two basic approaches: (i) supervised and (ii) unsupervised learning. Supervised learning (SL) is a machine learning approach that is defined by its use of labelled datasets: (i) classification of the data (4) and (ii) regression algorithm (5). In supervised learning, the algorithm “learns” from the training dataset by iteratively making predictions on the data and adjusting for the correct answer by upfront human intervention to label the data appropriately, to understand the relationship between dependent and independent variables. Unsupervised learning (U-SL) algorithms to analyze and cluster unlabeled data sets. These algorithms discover hidden patterns in data without the need for human intervention: (i) clustering, (6) (ii) association, (7) (iii) dimensionality reduction (8). Classifying big data can be a real challenge in supervised learning, but the results are highly accurate and trustworthy. In contrast, unsupervised learning can handle large volumes of data in real time. But there is a lack of transparency into how data is clustered and a higher risk of inaccurate results. This is where semi-supervised learning comes in... Semi-supervised learning (S-SL) is a happy medium, where you use a training dataset with both labelled and unlabeled data. It’s particularly useful when it’s difficult to

<sup>3</sup> //www.ibm.com/cloud/blog/ai-vs-machine-learning-vs-deep-learning-vs-neural-networks

<sup>4</sup> //www.ibm.com/cloud/learn/deep-

extract relevant features from data — and when you have a high volume of data ... it is an efficient processing of DNN<sup>5</sup>”.

**The method of investigation proposed in the project belongs to a semi-supervised learning, based on Learning Deep fluid mechanics applied to the modelling of interfaces (9).**

“Using Artificial Intelligence to Augment Human Intelligence by creating user interfaces which let us work with the representations inside machine learning models, we can give people new tools for reasoning”<sup>6</sup> ... indeed, but we are looking differently: **Augment by training Human Intelligence to create and to use efficiently the Artificial Intelligence (10).**

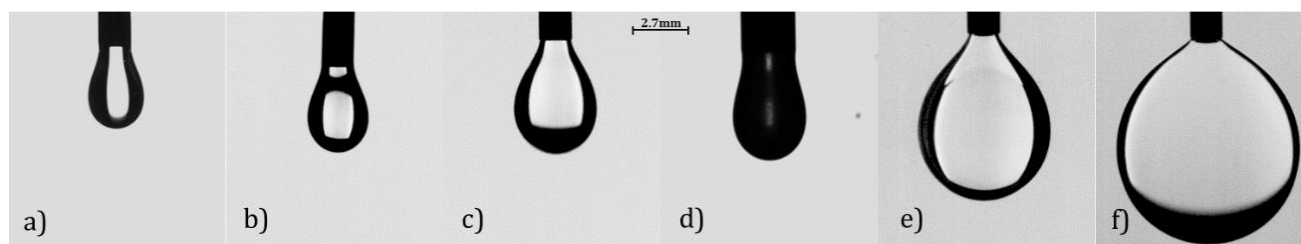
There are three objectives of the project:

O1. Implement in the REOROM group the training Learning Deep method based on the structure of AI semi-supervised learning algorithm, Table 1.

O2. Apply the LD method to establish the relation between the interface breakup/dynamics and the rheological properties of the fluids; to correlate the imagines of interface’s evolution with the rheological data and the numerical simulations, see (1).

O3. To create an image processing algorithm specialized for the analysis of flow visualizations, which is expected to be completed and extended in the framework of ML and DNN applications.

In the context of the project we propose a *benchmark problem*: Determining the fluid properties<sup>7</sup> using the image analysis – case of study: flow through a needle of fluid A immersed in the fluid B.



Question: How many input data/labels are needed to determine exclusively by image analysis the viscosity and the interfacial tension of fluid A?

The method of investigations is presented in Table II.1, where is also shown the corresponding between the steps in the proposed Learning Deep method and the characteristics of the DL-algorithms.

<sup>5</sup> Delua J., //www.ibm.com/cloud/blog/supervised-vs-unsupervised-learning

<sup>6</sup> Carter S., Nielsen M., 2017, <https://distill.pub/2017/aia/>: see also: Nielsen M., *Neural Networks and Deep Learning* (2015) Determination Press (free online book), Nielsen M., Chuang I.L. (2011) *Quantum Computation and Quantum Information*, Cambridge Univ. Press (one of the ten most highly cited works ever in physics).

<sup>7</sup> a) oil1/air; b) oil2/air; c) water/air; d) saliva/air; e) water/oil2; f) water/oil3.

**Table II.1.** Learning Deep vs. Deep Learning – steps, the work strategy, and methods **(10)**

No.	Learning Deep (layers of knowledge – work steps)	Deep Learning
I.1	Theoretical 1: Complex fluids, Interfaces, Rheology, CFD – numerical simulations <i>ANSYS Fluent</i> - <b>INPUT</b>	the depth of layers in a neural network <b>(2)</b> .
I.2	Experimental 1: Rheometry of the samples, Flow Visualizations in confined geometries - <b>INPUT</b>	
I.3	<i>Benchmark problem investigation (image processing of droplet formation and correlation with fluids rheology)</i>	
<b>I.4</b>	<b>Image processing: air-fluid dynamics of the interface related to the fluid rheology in the tested geometry (i.e. trachea model) (OUTPUT)</b>	
I.1.1	Theoretical 2: Hydrodynamics stability, Continuum mechanics, Turbulence – <b>(1)</b> , Stochastics, Differential geometry of surfaces and curves in space	hidden layers <b>(3)</b>
I.2.1	Experimental 2: Corroborate direct flow visualizations with the image processing; develop MATLAB code to trace/draw the interface from the images and to transfer the resulting geometry in the Fluent code.	
I.3.1	Analysis of the input parameters in relation to the errors in drawing the interface and in the prediction of the fluid rheology.	
I.4.1	Data analysis: Interface dynamics in the investigated domains – correlation between experiments, fluid rheology and numerical simulations of the flow.	
<b>Supervised learning</b>		<b>Supervised learning</b>
II.1	Classification and labelling: (i) literature from the domain, (ii) fluids as function of their rheology; (iii) visualization techniques, (iv) flow domains and boundary conditions, (v) corroboration with numerical simulations	(i) classification of the data <b>(4)</b>
II.2	Techniques and algorithm to fit the data (imagines contour); (i) fitting with solutions of equations by ORIGIN and <i>Mathematica</i> ; (ii) fitting using numerical codes MATLAB	regression algorithm <b>(5)</b> .
<b>Unsupervised learning</b>		<b>Unsupervised learning</b>
III.1	Clustering interfaces with similar topologies as function of: (i) flow domain, (ii) fluids rheology, (iii) images resolutions	(i) clustering, <b>(6)</b>
III.2	Labelling interfaces images as function of their topology	(ii) association, <b>(7)</b>
<i>Results from the specific applications are unified in one single Database</i>		
III.3	Relate the labels with the non-dimensional parameters and boundary conditions	(iii) dimensionality reduction <b>(8)</b> .
<i>Transfere in cloud a Database for the labelled and un-labelled images</i>		
III.4	Relate the image of the interface with the flow conditions	
<b>Semi-supervised learning (9) - OUTPUT</b>		
<b>IV</b>	<b>Correspondence – fluids rheology and interface’s topology</b>	<b>ML-DNN algorithm</b>

### Experimental and numerical investigations of air-ways flows in the presence of mucus (part I)

The main scientific responsibilities of the UPB partner in MUCCA project the are presented in the Work Plan 5 (WP5) from the proposal: Use-case MED-2 (xAI in the diagnostic of pulmonary, tracheal, and nasal airways):

Description	Year 1				Year2				Year3			
	Q1	Q2	Q3	Q4	Q1	Q2	Q3	Q4	Q1	Q2	Q3	Q4
<b>WP5 MED-2</b>												
T 5.1 Reconstruction on tomographic scans												
T5.2 Experiments and validation on air-mucus in idealized geometries												
T5.3 Experiments and validation on air-mucus in respiratory geometries												
T5.4 Test of xAI on simulation results												

<b>WP5</b>	<b>MED-2</b>	<b>1</b>	<b>36</b>					
<b>Contribution of project partners</b>								
Partner number	1	2	3	4	5	6	7	8
Total effort per partner (Person.months)	1.8			18	<b>25.2</b>			
<b>Aim of the WP</b>								
The aim of the WP is to test the xAI methodology in a complex physiological system given by the respiratory system (upper and lower tracts). To test xAI in nasal and pulmonary operating conditions it will be necessary to consider the geometric airway intricacy and the passage of air. In a subset of cases, we will analyse the concurrent passage of air and mucus, causing large resistances and non-linear response. In order to capture the complex phenomenon of breathing, the WP will analyse the visco-elastic rheological response of mucus in experiments on idealized geometries and derive a non-Newtonian constitutive model to be used in simulations of breathing in more complex anatomical geometries.								
<b>Tasks</b>								
<b>T5.1</b>	<b>Reconstruction of tomographic scans (M1 – M6; responsible: 5, involved partner: 5). Reconstruction of respiratory tracts, using MedLea software products DigiScan. Staff: PI-5. Role of the participants: analysis.</b>							
<b>T5.2</b>	<b>Experiments and validation on air-mucus in idealized geometries (M7 – M12; responsible: 4, involved partner: 4+5). Experiments about flow in a number of idealized geometries. Rheological comparison with simulation performed by Medlea to optimize the model both at analytical level and by proper numerical treatment. Staff: PIs of Partner 4 and 5 + collaborators. Role of the participants: data preparation, analysis.</b>							
<b>T5.3</b>	<b>Experiments and validation on air-mucus in respiratory geometries (M13 – M18; responsible: 4, involved partner: 4+5). Experiments with usage of multi-branched geometries and simulations using the software product WeResp by Medlea. Preparation of a database of results to be used for xAI. Staff: PIs of Partner 4 and 5 + collaborators. Role of the participants: experiments, analysis, samples preparation.</b>							
<b>T5.4</b>	<b>Test of xAI on simulation results (M19 – M36; responsible: 4, involved partner: 1+4+5). Test of state-of-the-art and new xAI deployed by WP7 to predict the global airflow resistances in respiratory conduits. Assessment of causal relations between predictions and simulation results with xAI. Staff: PIs of Partner 4 and 5 + collaborators. Role of the participants: analysis, sample preparation.</b>							
<b>Deliverable</b>	<b>Month of delivery</b>	<b>Title of deliverable</b>						
<b>D5.1</b>	6	First group of reconstructed patient nasal and respiratory anatomies from CT scans.						
<b>D5.2</b>	12	Characterization of the mucus-air rheology in bulk and confined regions. Anatomical reconstructions completion.						
<b>D5.3</b>	18	Validated air-mucus flows in idealized and multibranched conduits. Database to be used for xAI follow-on.						
<b>D5.4</b>	27	Prototype of the xAI algorithm implementation.						
<b>D5.5</b>	36	Best performing XAI and assessment of the causal relations producing best and worst predictions.						

## Introduction

The first-year report presents the results related to the Task 5.1 and 5.2 from the project proposal. The main goals of this research stage were the following:

1. To establish the procedure to extract from CT image the test geometry, to reconstruct the test geometry for the experiments, to perform qualitative visualizations and numerical simulations of the air flow in the confined domains (which corresponds to some test geometries).
2. To design the test setup and to make the acquisition of the necessary equipment for the experiments scheduled in the second-year of the project;
3. To find the best sample for the synthetic mucus sample, to characterize its rheology and to establish the material constitutive relation to be implemented in the numerical simulations.

The first-year achievements are satisfactory. One can say that results are „on the line” with the proposed tasks. Hence, there are fulfilled the conditions to produce quality data from the CFD investigations and analysis, which are scheduled for the next year.

There are two unfulfillments of the first year, mainly generated by the pandemic situation:

1. The cooperation with MedLea partner didn't reach yet the optimum. There were obtained promising results but up to now we do not have a full understanding of the original code produced by our partner. This was to some extent expected since the knowledge transfer cannot be optimal using only the on-line contacts. We plan a working visit of two PhDs from my group at MedLea in the first semester of the next year (hoping that access conditions in the institutions will be back to normal).
2. The acquisitions of the equipment (optics for visualizations, components, and transducers for the setup) were delayed. Therefore, the experimental investigation of the air flow in the geometry was limited to qualitative visualizations. However, at the beginning of December we expect to receive all necessary devices to perform the tests accordingly to the timetable of the task T5.3. It is important to remark that the access of the team's members in the laboratory was restricted for some periods of the year, which of course produced undesired breaks in our work.

In this first stage of the project we defined **the benchmark problem**: *Image processing of droplet formation and correlation with fluids rheology*, and the activities related to this associated research project have started, see Tab. II.1 (I.3, I.2.1) and the Annex A.II.4.

## II. 1 – Task T5.1 Reconstructions of the analyzed respiratory airways from CT

The first bifurcation of trachea was chosen as the test geometry. The procedure to obtain the corresponding geometry used in experiments and numerical simulations (see Fig. II.1) is presented in the Annex A.II.1. One considers that task T5.1 was achieved, and the procedure of images reconstruction can be implemented in a AI-algorithm (step I.2.1 in Tab. II.1).

From CT scan to 3D model: step-by-step guide (Annex A.II.1)

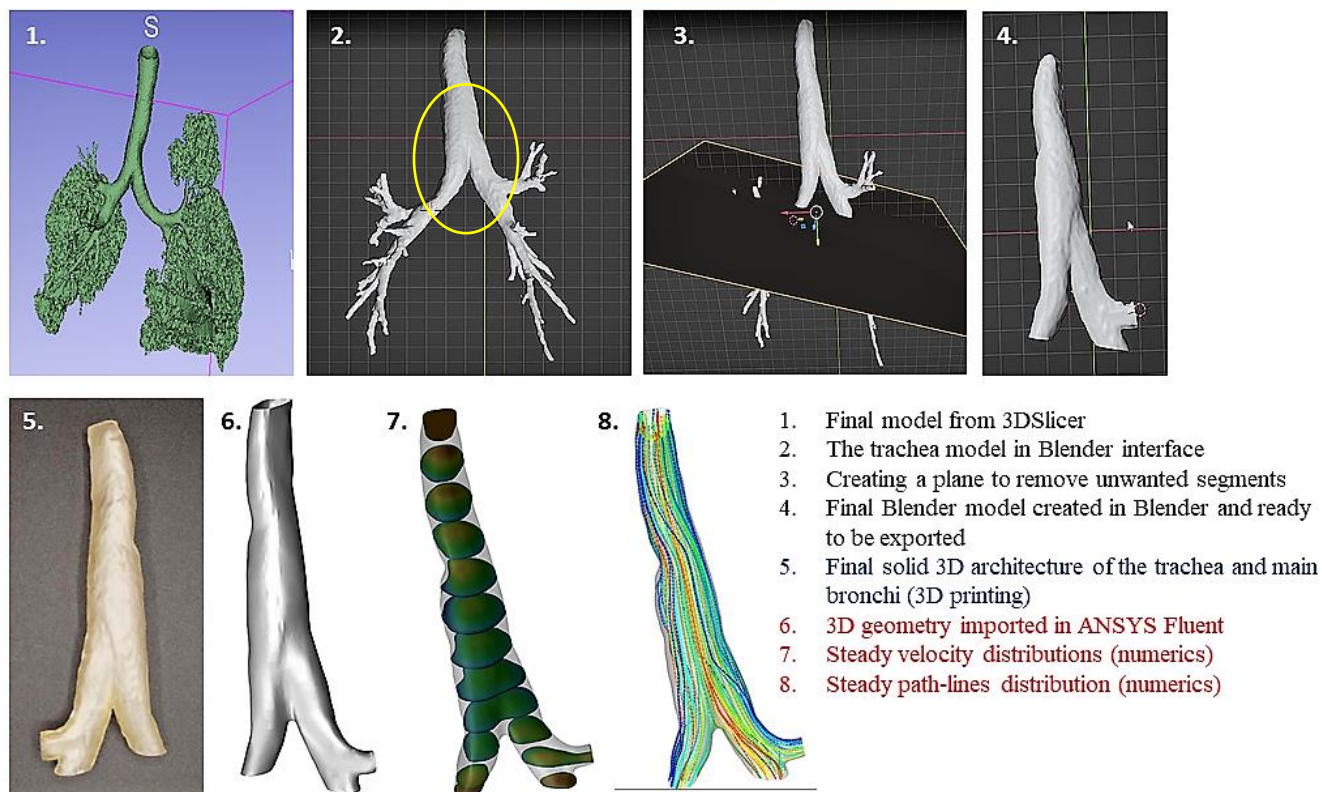


**Figure II.1** From CT to physical geometry and numerical simulations; case of study: the first bifurcation of trachea. The geometry marked in image 2 is reconstructed in image 4; it is the test domain (i.e. the interior of the physical body from image 5), with the same dimensions as the 3D geometry used for numerical simulations (images 6-8).

## II. 2 – Task T5.2 Experiments and validation on air-mucus in idealized geometries

### II.2.1 – Manufacture of the test geometries and flow visualizations of the gel transport

The 3D test geometries are obtained by 3D printing (see A.II.1), Fig. II.2. The idealized planar geometries are manufactured using a 3D printed profile fixed between two transparent (glass or plastic) planar surfaces, Fig. II.3. The idealized 3D transparent geometries are produced by PDMS cast method, Fig. II.4. One face of the PDMS geometry is a planar transparent glass surface to avoid the light reflections of the laser beam used in the PIV method. The visualizations of the gel transport in the PDMS geometry under an oscillatory air flow are shown in Fig. II.5.

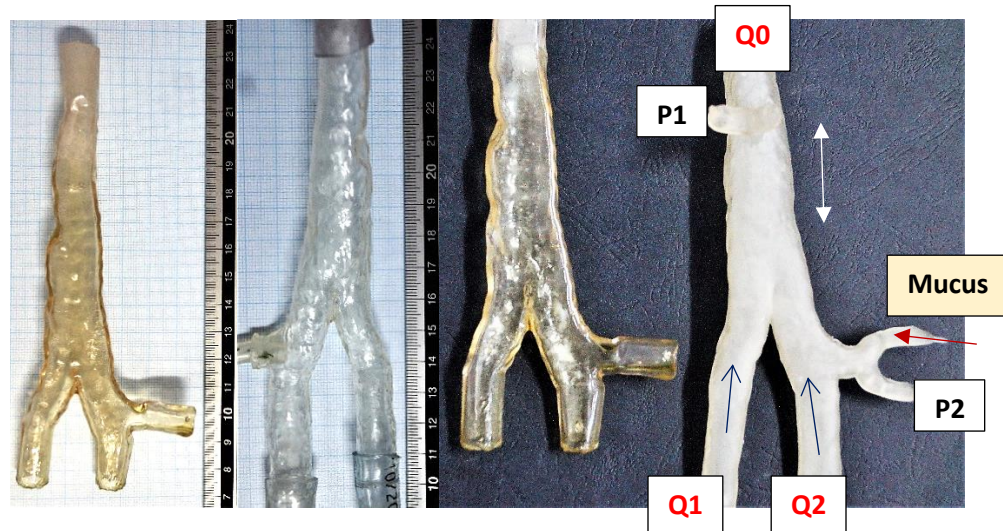


**Figure II.2** 3D test geometries with different degree of transparency (positions of transducers are marked: P1-2 – pressure transducers, Q1-2, Q0 – air flow rate transducers). The thickness of the walls’ body is ~1 mm.

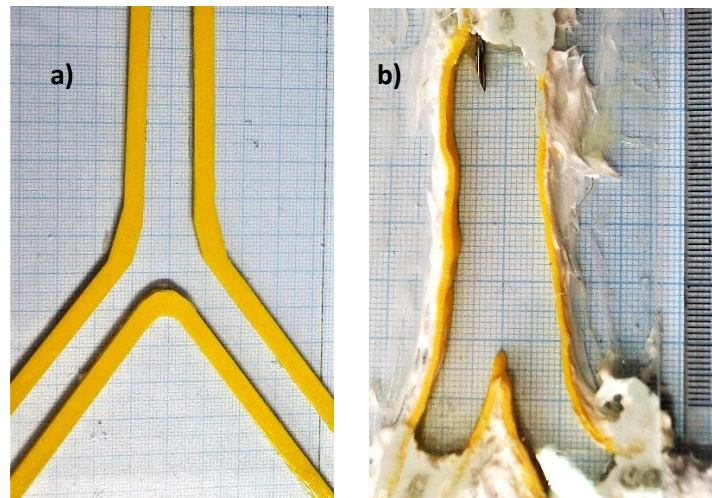


**Figure II.3** Idealized planar test geometries: a) symmetric test geometry, b) real contour of the median plane of the 3D test bifurcation from Fig. II.2 (2 mm thickness).

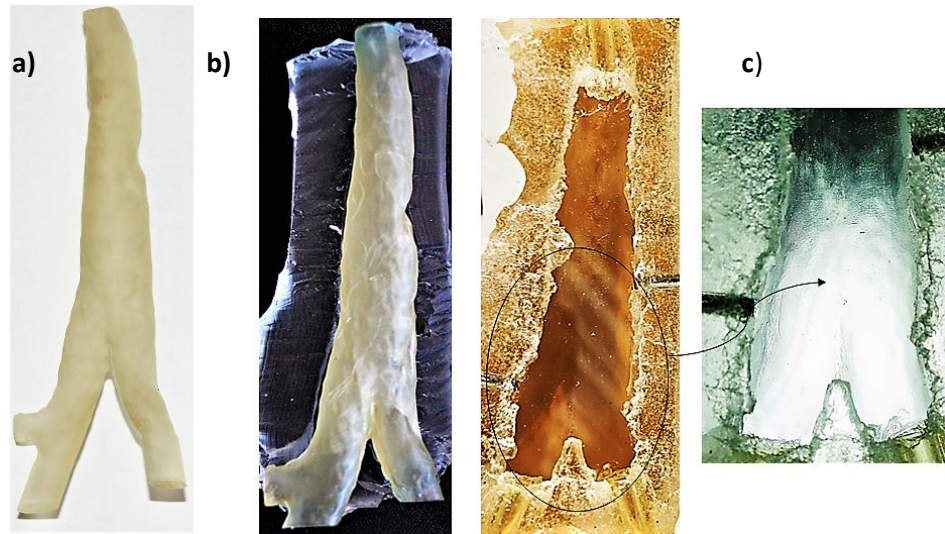


**Figure II.4** The PDMS geometry: a) mold of the test geometry (the interior of the bodies from Fig. II.2, same dimension with Fig. II.1.4, b) PDMS cast method, c) PDMS test geometry (with one glass transparent face).

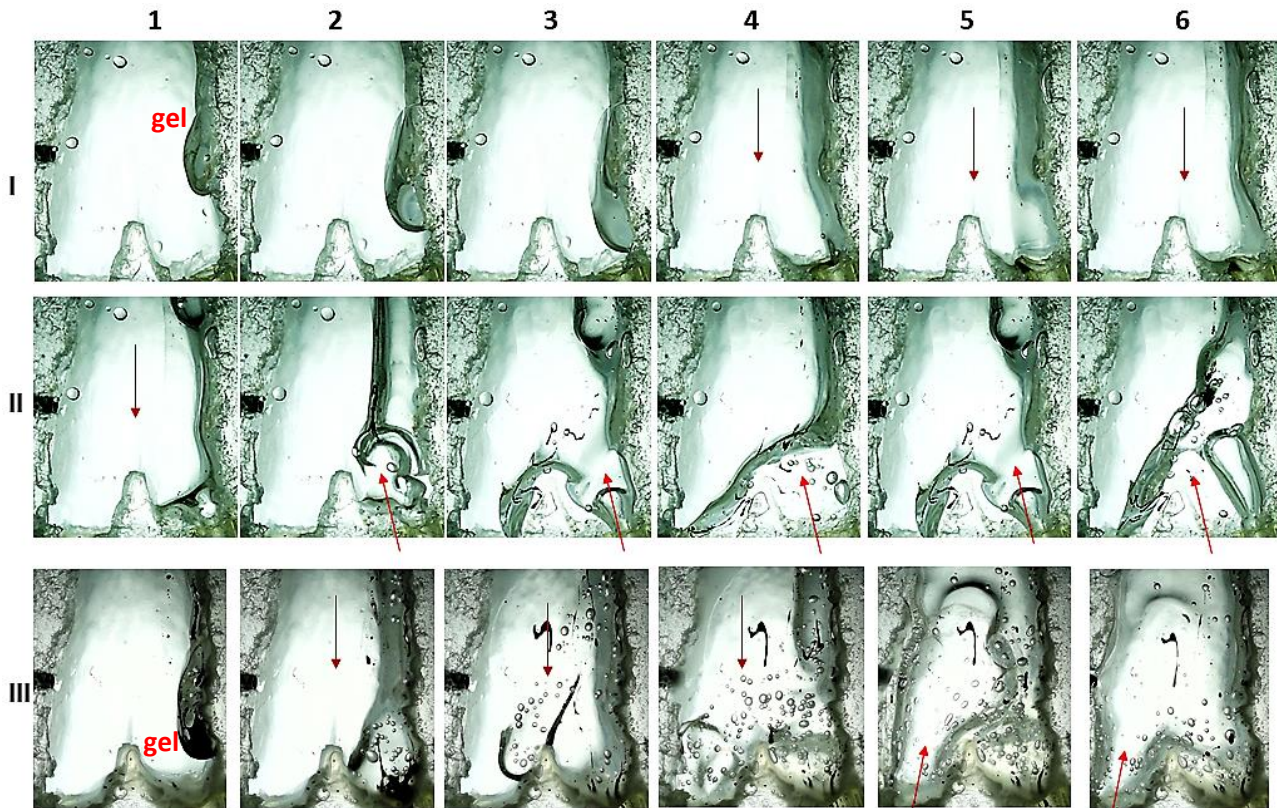


**Figure II.5** Direct visualizations of the gel (mucus like sample) in the transparent PDMS geometry (Fig. II.4.c) under oscillatory air flow (test 1, I-II; test 2, III; air direction are indicated by arrows). At the end of the oscillatory cycle the gel sample plugs under the air flow almost completely the two minor bifurcations of the geometry.

There were analyzed some setups used to perform experiments of the air flow in trachea, Fig. II.6 and Fig. II.7. The scheme of the proposed setup is shown in Fig. II.8. Under our knowledge, no experimental visualizations of the air flow in the presence of mucus in trachea were published.

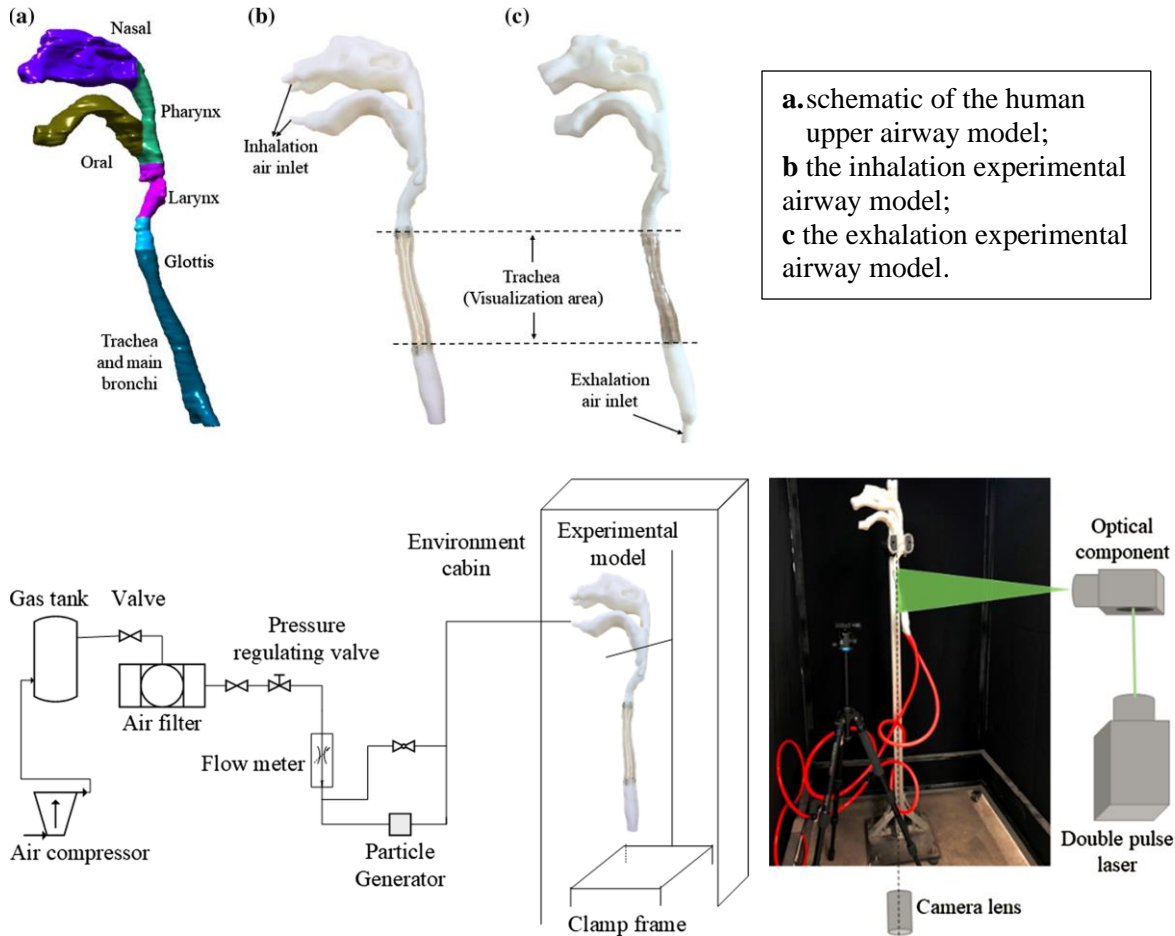


**Figure II.6** Trachea model and the experimental setup in a close cabin<sup>8</sup>.

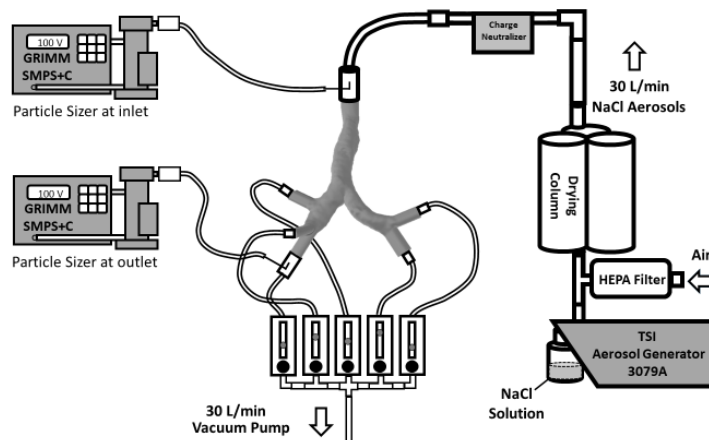


**Figure II.7** The experimental setup of nanoparticle lung deposition measurements<sup>9</sup>.

<sup>8</sup> Xu X. et al. (2020) *Investigation of inhalation and exhalation flow pattern in a realistic human upper airway model by PIV experiments and CFD simulations*, Biomechanics and Modeling in Mechanobiology, 19 (1), Springer

<sup>9</sup> Ma L. et al. (2020), *A Combined Computational and Experimental Study on Nanoparticle Transport and Partitioning in the Human Trachea and Upper Bronchial Airways*, Aerosol and Air Quality Research, 20: 2404–2418.

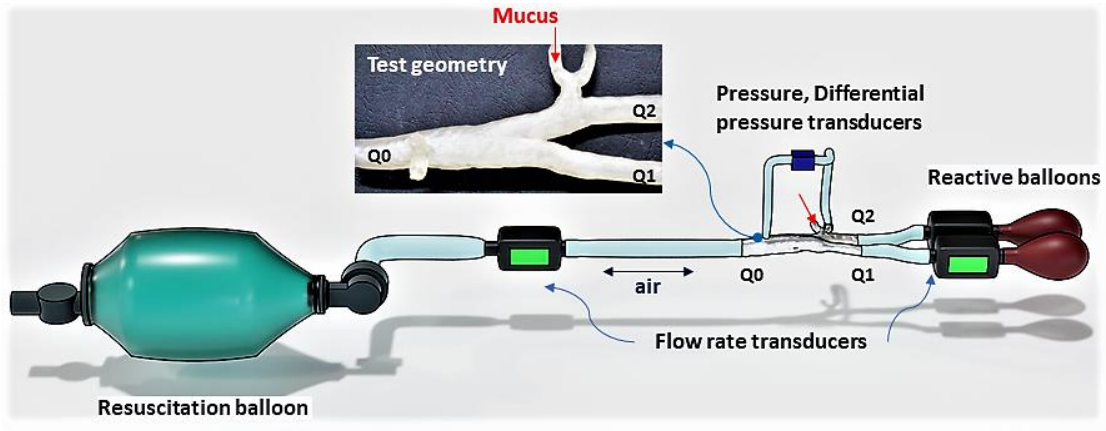


**Figure II.8** The proposed setup (already tested in the absence of transducers).

**II.2.2 Characterization of the mucus rheology**

Despite that mucus composition/rheology is strong dependent of the type/stage of diseases and the particular human/patient physiological/pathological conditions, all the studies reveal that rheology of the human/synthetic mucus<sup>10</sup> is similar to a gel characterized in oscillatory shear test as an *elastic gel* with  $G' > G''$ , where  $G'$  is the elastic (storage) modulus and  $G''$  is the viscous (loss) modulus, see Fig. II.9.

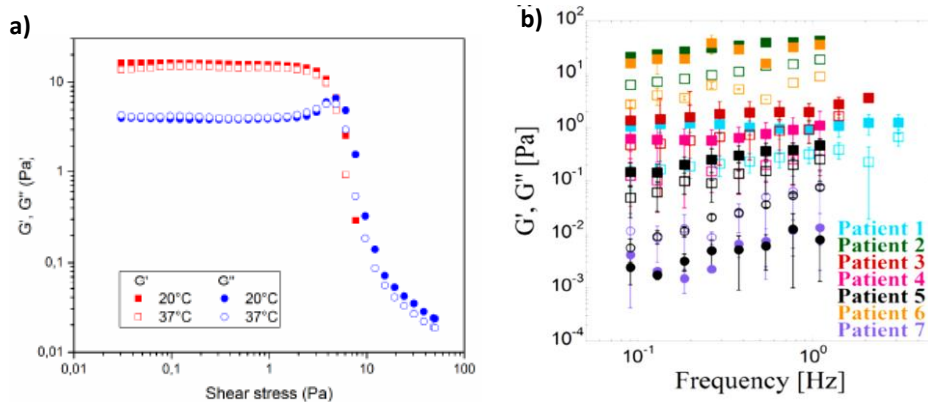


**Figure II.9** a) Oscillatory test at constant frequency and strain/shear stress sweep test<sup>10,3</sup>, b) Dynamics moduli as function of frequency at constant strain/stress amplitude<sup>10,2</sup>.

The elastic gels ( $G' > G''$ ) are characterized by the following rheological properties: (i) the dynamics moduli are almost parallel in the frequency sweep test, (ii) strong shear thinning behavior (viscosity is decreasing with frequency/shear rate), (iii) the presence of a yield state, i.e. the gel has a fluid like behavior

<sup>10</sup> Loiseau E. et al. (2020) *Active mucus-cilia hydrodynamic coupling drives self-organization of human bronchial epithelium*, Nature Physics 16, 1158-1164; Jory M. et al. (2019) *Mucus microrheology measured on human bronchial epithelium culture*, Frontiers in Physics 7, art. 19; Lafforgue O. et al. (2018) *Rheological properties of synthetic mucus for airway clearance*, J. Biomed. Mat. Research Part A 106(2), 386-396; Chen Z. et al. (2019) *Determination of rheology and surface tension of airway surface liquid: a review of clinical relevance and measurement techniques*, Respiratory Research 20:274; Levy R. et al. (2014) *Pulmonary fluid flow challenges for experimental and mathematical modeling*, Integ. Comp. Biology 54(6), 985-1000.

at a yield value of the applied shear stress  $\sigma_0 > 0$ . The synthetic or artificial mucus fabricated and investigated in the laboratories disclose such rheology, which is considered to be similar with the real mucus. However, the mucus rheology is not only dependent on the chemical initial composition, but also on its contact with oxygen and the concentration of air bubbles in the bulk. It is difficult to create for investigations an artificial mucus (rheological similar with the real one) with controlled and stable properties, since the measurement *in vitro* with real mucus disclose a large range for viscosity ( $\eta$ ) or elasticity ( $G'$ )<sup>10,5</sup>, see also Fig. II.9.b:  $0.1 < \eta < 50$  Pas,  $0.1 < G' < 200$  Pa, respectively.

The main studies (relevant for the pathology) are focused to the correlation of the mucus rheology with its behavior in the vicinity of the epithelium<sup>10,1-3</sup>, with its rupture and transport in the human airways<sup>11</sup>. There are not accurate studies dedicated to the correlation between shear and extensional properties of the mucus, in relation to the modeling of mucus transport in airways in similar physiological conditions.

The sample prepared for our first investigations (SAM – Sample Artificial Mucus) is a solution based on water (as solvent) and the food thickener Fresubin, produced for medical use by Fresenius Kabi company (as solute), Fig. II.10.

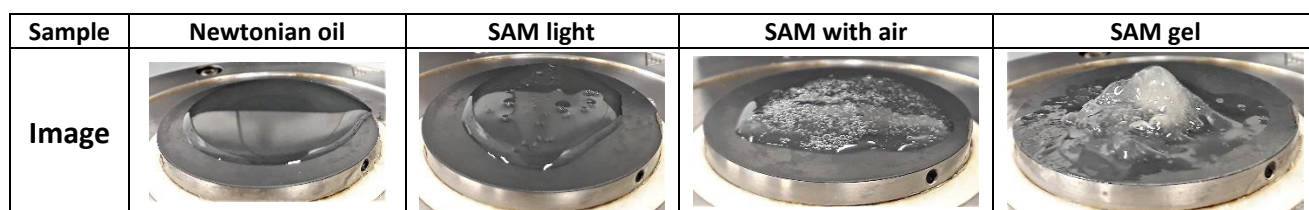


**Figure II.10** The aspects of the samples before the shear experiments: Newtonian oil, SAM light (transparent), SAM with air bubbles, SAM with undissolved solute (gel like).

We investigated the SAM rheology as function of thickener concentration, presence of air bubble and time degradation at 25° C using the MC 301 Anton Paar rheometer (rotational cone-plate configuration, oscillatory frequency sweep at 0.1 [-] strain amplitude). The results are shown in Figs. II.11.

For the next investigations we choose as a reference the sample 1g/50 ml – III (sample 1g/50ml – II with air bubbles). This sample discloses similar rheological properties as the synthetic or real mucus samples<sup>8,9</sup> used in some published works, Fig. II.12.

<sup>11</sup> Yi H. et al (2021) *Computational analysis of obstructive disease and cough intensity effects on the mucus transport and clearance in an idealized upper airway model using the volume of fluid method*, Phys. Fluids 33, 021903; Hu Y. et al. (2015) *A microfluidic model to study fluid dynamics of mucus plug rupture in small lung airways*, Biomicrofluidics 9, 044119.

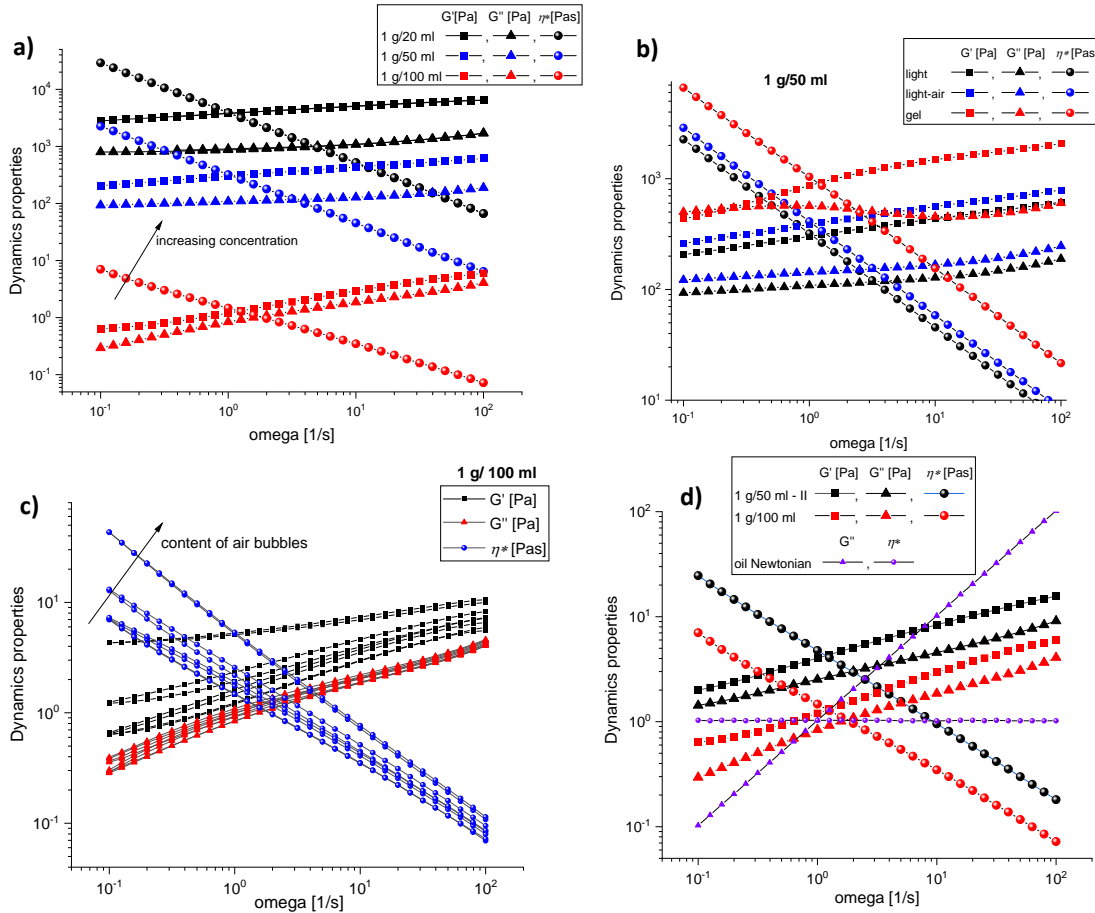


**Figure II.11** a) Influence of thickener concentration, b) Influence of the bubbles and not complete mixing in comparison to the SAM light (transparent) sample, c) influence of air bubbles, d) SAM samples in comparison to a pure Newtonian oil (used for calibration). Here 1g/50ml – II is the sample 1g/50 ml (light) tested after 1 day from the mixing.

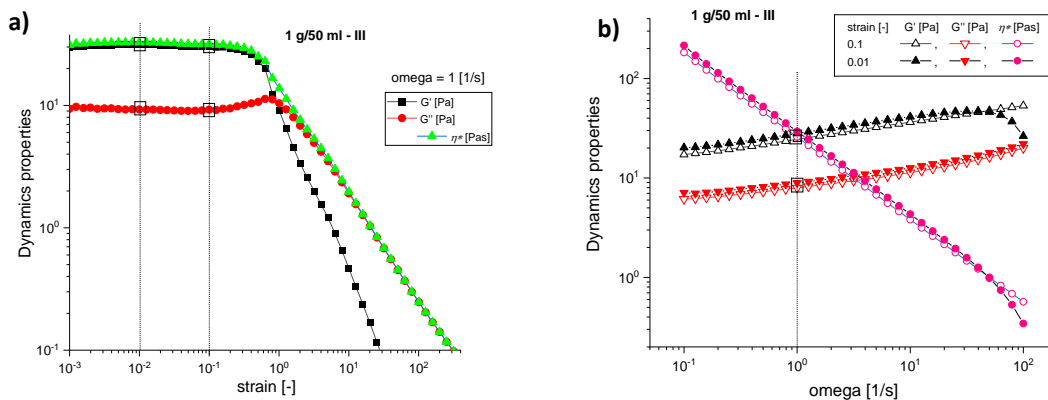


**Figure II.12** a) in the strain sweep test  $G' > G''$ , the moduli are parallel up to a strain amplitude of 0.1 (which corresponds to a shear stress amplitude of 3.2 Pa) and  $G''$  discloses a maximum at the end of the linear regime, before the thinning domain (typical rheological behavior for soft solids/gels), see Fig. II.9.a; b) In the frequency sweep test the dynamics moduli are parallel,  $G' > G''$ , and their values are in the range 0.5 Pa to 30 Pa (see Fig. II.9.b)

In Fig. II.13 are shown the viscosity curves for the samples 1g/50 ml – II and – III. The presence of air bubbles in sample III not just increases the viscosity, but also generate a difference between the complex viscosity -  $\eta^*(\omega)$  and the shear viscosity -  $\eta(\dot{\gamma})$ , Fig. II.13.b (which is not the case for the sample II, Fig. II.13.a). This rheological characteristic is typical for emulsions.

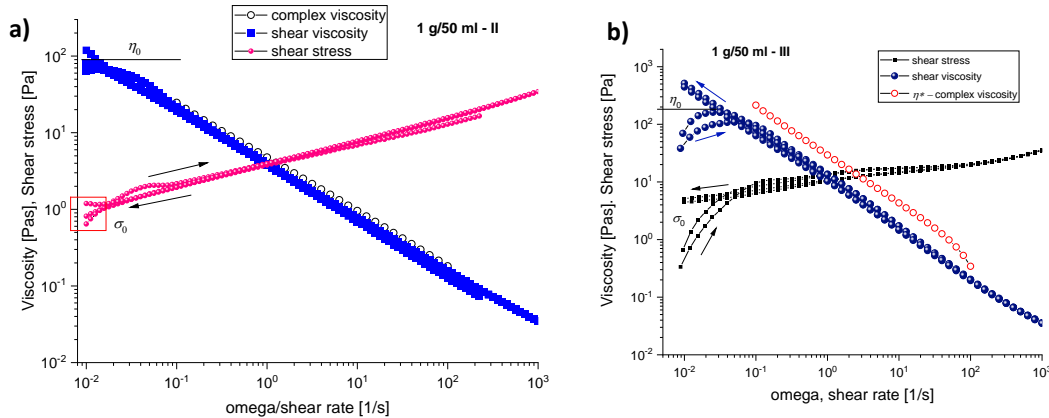


**Figure II.13** Flow curve (shear stress -  $\sigma$  vs. shear rate -  $\dot{\gamma}$ ) and the viscosity functions,  $\eta(\dot{\gamma})$  and  $\eta^*(\omega)$ , for the samples 1g/50 ml – II (a) and 1g/50 ml – III (b). Both samples disclose an apparent yield stress -  $\sigma_0$ .

Mucus discloses rheological characteristics of viscoelastic fluids with yield stress (some author consider these fluids as belonging to the category of viscoplastic materials<sup>12</sup>). The yield state characterizes the transition from the solid rheological behavior to the fluid one. The onset of flow is determined if the critical yield state ( $\sigma_0, \dot{\gamma}_0, \gamma_0$ ) is achieved during the loading and deformation of a soft solid<sup>13</sup>. Here  $\sigma_0$  is the yield shear stress,  $\dot{\gamma}_0$  is the yield strain rate and  $\gamma_0$  is the yield strain, respectively. In general, the yield stress fluids are also viscoelastic fluids, but in a first approximation they are modelled with a generalized Newtonian constitutive relation, where the extra-stress tensor  $\mathbf{T}_E$  has the expression:  $\mathbf{T}_E = 2\eta(\dot{\gamma})\mathbf{D}$ , where  $\eta(\dot{\gamma})$  is the viscosity function and  $\dot{\gamma}$  is the second invariant of the stretching  $\mathbf{D}$ .

There are many models for the viscosity function of the yield stress fluids and almost all of them incorporate the yield shear stress or the yield shear rate as parameters<sup>14</sup>.

<sup>12</sup> Larson R.G. (1999) *The structure and rheology of complex fluids*, Oxford Univ Press; Coussot P. (2014), *Yield stress fluid flows: A review of experimental data*, J. Non-Newt. Fluid Mech. 211, 31–49.

<sup>13</sup> Malkin A. et al. (2017) *A modern look on yield stress fluids*, Rheol Acta 56, 177–188; Coussot P. (2018) *Slow flows of yield stress fluids: yielding liquids or flowing solids?*, Rheol Acta 57, 1–14.

<sup>14</sup> Balmforth N.J. et al. (2014) *Yielding to stress: Recent developments in viscoplastic fluid mechanics*, Annu. Rev. Fluid Mech. 46, 121- 146; Mitsoulis E., Tsamopoulos J. (2017) *Numerical simulations of complex yield-stress fluid flows*, Rheol Acta 56, 231–258; Saramito P., Wachs A. (2017) *Progress in numerical simulation of yield stress fluid flows*, Rheol Acta 56 (3), 211-230; Fragedakis D et al. (2016) *Yielding the yield stress analysis: A thorough comparison of recently proposed elasto-viscoplastic (EVP) fluid models*, J. Non-Newt. Fluid Mech. 236, 104-122; Saramito P. (2019) *A new elastoviscoplastic model based on the Herschel–Bulkley viscoplastic model*, J. Non-Newt. Fluid Mech. 158 (2019) 154-161.

The origin of all these constitutive relations is the Bingham relation, extended for shear thinning fluids by Herschel-Bulkley (HB) models<sup>14,4-5</sup>. The classical yield stress fluid models are valid only if the local shear stress is beyond  $\sigma_0$ . Below this threshold value the material is defined by a solid constitutive relation, so the viscosity is going to infinite in this domain (as it is in the classical Bingham model). This rheological behavior is not acceptable, especially if the numerical simulations are performed<sup>14,2-3</sup>. Therefore, the yield stress fluid viscosity is regularized, in the sense that for  $\sigma < \sigma_0$ , or  $\dot{\gamma} < \dot{\gamma}_0$ , the material behaves as a Newtonian fluid with high viscosity<sup>15</sup>.

In relations (1) and (2) are given two HB models (implemented in the commercial Fluent code) with regularization of the viscosity:

$$\sigma = \sigma_0 + k \left( \frac{\dot{\gamma}}{\dot{\gamma}_0} \right)^{n-1} \dot{\gamma}, \quad \dot{\gamma} > \dot{\gamma}_0 \quad (1.1)$$

$$\sigma = \left[ \sigma_0 \frac{2-\dot{\gamma}/\dot{\gamma}_0}{\dot{\gamma}_0} + k((2-n) + (n-1)\dot{\gamma}/\dot{\gamma}_0) \right] \dot{\gamma}, \quad \dot{\gamma} < \dot{\gamma}_0; \quad (1.2)$$

and

$$\sigma = \sigma_0 + k[\dot{\gamma}^n - \dot{\gamma}_0^n], \quad \sigma > \sigma_0, \quad (2.1)$$

$$\sigma = \frac{\sigma_0}{\dot{\gamma}_0} \dot{\gamma}, \quad \sigma < \sigma_0, \quad (2.2)$$

where  $n < 1$  is the flow index (shear thinning/pseudoplastic behavior) and  $k$  is a parameter called consistency.

Another possibility to model a yield stress fluid is to consider a plateau in the flow curve  $\sigma = \sigma(\dot{\gamma})$ , the value of the plateau being considered the yield shear stress. Some of the generalized Newtonian models (which do not contain explicitly the yield parameters) are proper for such modelling<sup>16</sup>. Relation (3) defines the flow curve (and implicit the viscosity function) of the Carreau model:

$$\sigma = \left[ \eta_\infty + (\eta_0 - \eta_\infty) \cdot (1 + (\lambda\dot{\gamma})^2)^{\frac{n-1}{2}} \right] \dot{\gamma}, \quad (3)$$

represented in Fig. II.14 for  $n = 0$  and  $n = -1$  (here  $\eta_0$  and  $\eta_\infty$  are the zero and infinite shear viscosities and  $\lambda$  is the time parameter).

<sup>15</sup> Frigaard I.A., Nouar C. (2005), *On the usage of viscosity regularization methods for visco-plastic fluid flow computation*, J. Non-Newt. Fluid Mech. 127 (1), 1-26; Syrakos A. et al. (2014) *Performance of the finite volume method in solving regularized Bingham flows: Inertia effects in the lid-driven cavity flow*, J. Non-Newt. Fluid Mech. 208/209, 88-107.

<sup>16</sup> Larson R.G. (1992) *Instabilities in viscoelastic flows*, Rheol. Acta 31, 213–263; Balan C. (2001) *Experimental and numerical investigations on the pure material instability of an Oldroyd's 3-constant model*, Continuum Mech Thermodyn 13, 399–414.

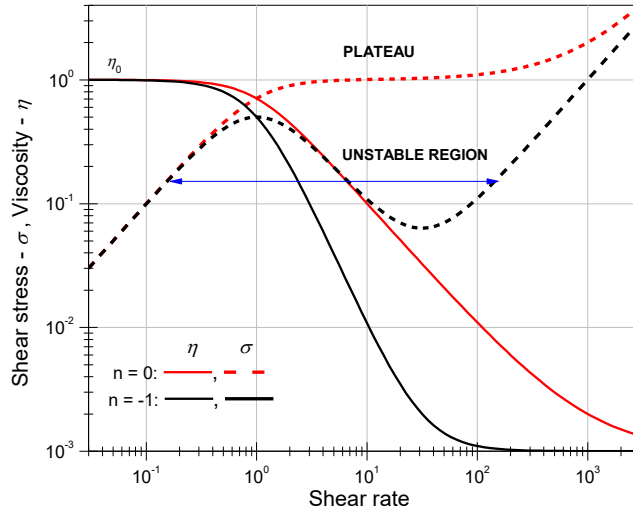


**Figure II.14** Flow curves and viscosity functions of the Carreau model at  $n = 0$  and  $n = -1$  ( $\eta_0 = 1$  Pas,  $\eta_\infty = 1$  mPas,  $\lambda = 1$ ).

At  $n = 0$  the Carreau relation discloses a relevant plateau, which can define the yield stress  $\sigma_0$ . At  $n = -1$  the same model discloses a non-monotonic flow curve, which is dynamically unstable. As consequence, a jump in shear rate will take place at a critical shear stress associated with the yield stress value.

The fitting of sample's 1g/50 ml – III shear viscosity with the models HB-1 (1) and Carreau (3) are represented in Fig. II.15.

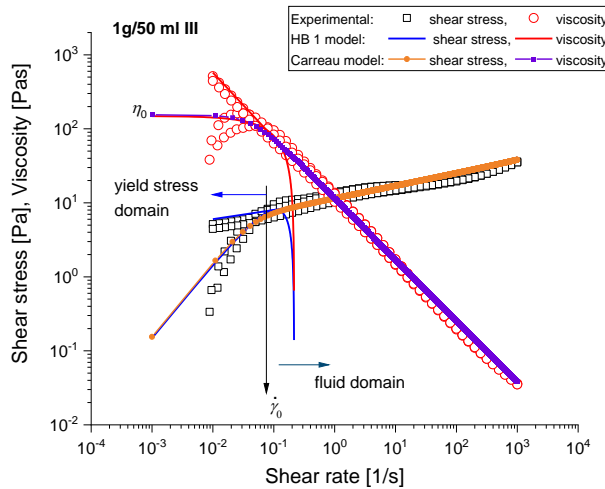


**Figure II.15** The fitting of the shear viscosity form Fig. b. with the HB-1 model ( $\sigma_0 = 3$  Pa,  $k = 50$  Pas,  $\dot{\gamma}_0 = 0.1$  s<sup>-1</sup>,  $n = 0.22$ ) and Carreau model ( $\eta_0 = 155$  Pas,  $\eta_\infty = 0.001$  Pas,  $\lambda = 23$  s,  $n = 0.17$ ).

The constitutive relations HB-1 and Carreau will be used to model (in the first approximation) the rheology of the mucus sample. Both relations give a fair representation in shear

of the sample’s rheology, but without to model the elasticity (since they are generalized Newtonian fluids). We anticipate that elongational tests (including determination of the surface tension) have to be performed in the future to obtain a more realistic mucus model. However, the implementation of viscoelasticity in the 3D numerics is a difficult mission.

### II.2.3 Numerical simulations of the air flows in the test geometries

The test geometry (see Figs. II.1-2) is presented in Fig. II. 16. The numerical solutions of the air flow are obtained using two numerical codes: (i) the commercial code Ansys Fluent (Ansys Workbench 2021 R1) and (ii) original *Moebius* developed by MedLea, our partner in the project.

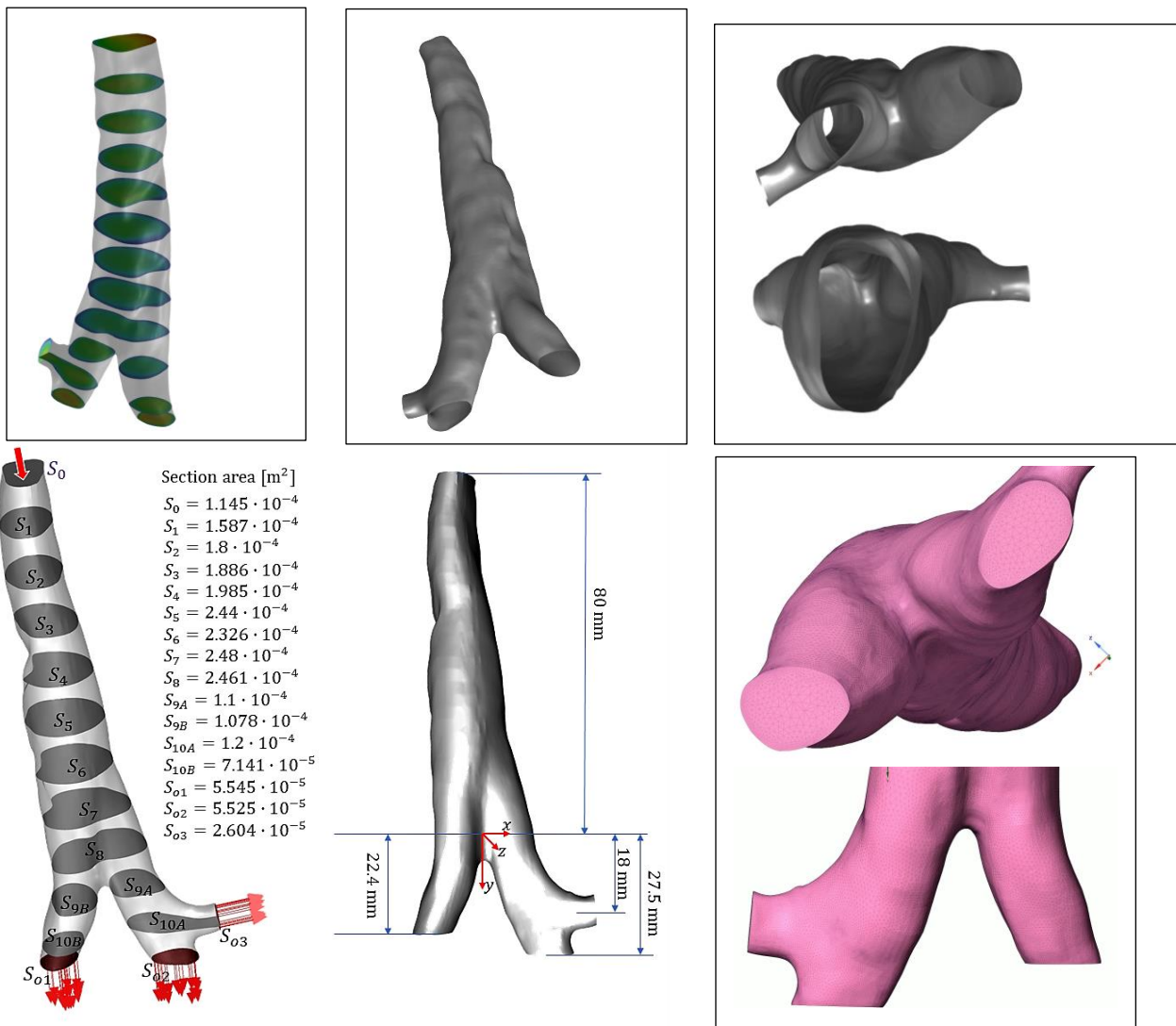


**Figure II.16** 3D test geometry (trachea’s first bifurcation), computation flow domain and dimensions. The geometry is obtained from the CT images and the model is fabricated using the 3D printing method (Fig. II.1-2).

Comparative numerical solutions are shown in the Annex II.2 for a test case: steady air flow with constant velocity of surface  $S_o$  and imposed constant pressure at the exist surfaces  $S_{o1}$ ,  $S_{o1}$  and  $S_{o1}$ . Same test case was also run for the idealized geometry from Fig. II.3 (pseudo-planar symmetric bifurcation). The run steps of the Moebius numerical code are presented in the Annex II.3.

Of course, the real expiration-inspiration cycle of air flow in the trachea is different. In Fig. II.17 is presented a flow rate and pressure variation of the air flow in a cycle during a period of 6.5 s.

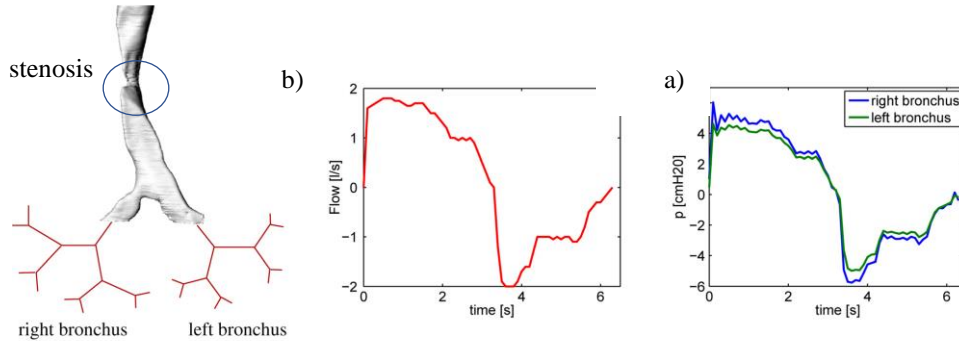


**Figure II.17** Flow rate variation (a) in the trachea with stenosis during a cycle expiration-inspiration given by the pressure distributions (b) at the exit of the geometry<sup>17</sup>.

The same cycle was tested for our geometry using the Ansys Fluent code with the following boundary conditions: the pressure at the inlet is  $p = 0$  (atmospheric pressure) and the variation of pressure at the outlets is unsteady,  $p = p(t)$ , given by the diagram from Fig. II.18.

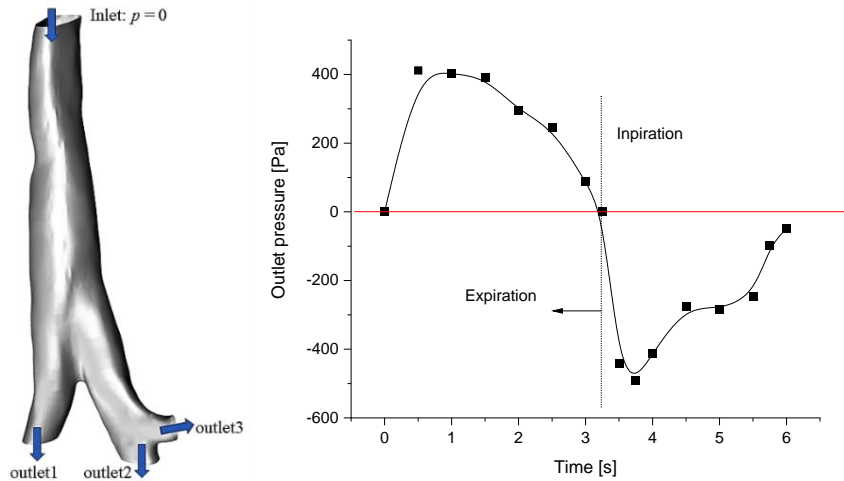


**Figure II.18** Boundary conditions for the unsteady air flow in the test bifurcation.

<sup>17</sup> Malve M. et al (2011) *FSI analysis of a human trachea before and after prosthesis implantation*, J. Biomech. Eng. 133(7), 071003

The computed velocity distributions during a cycle are shown in Fig. II.19.

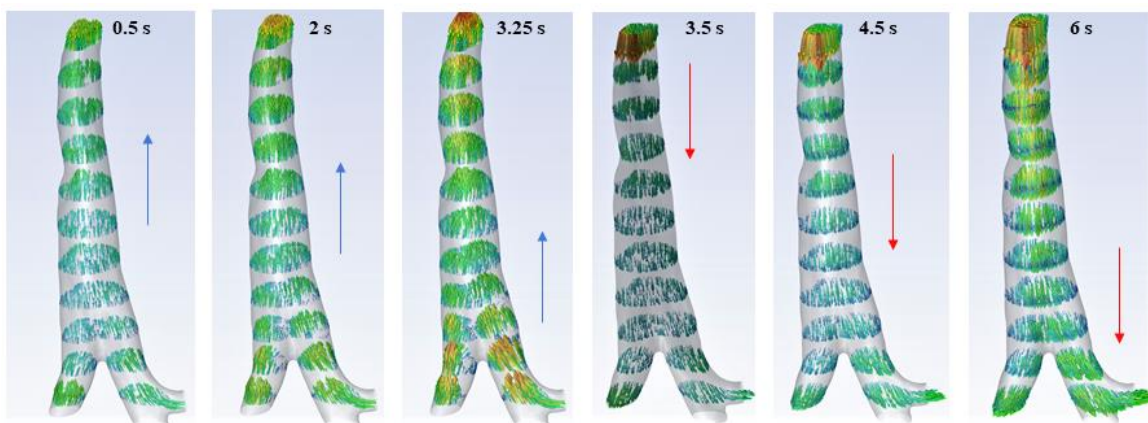


**Figure II.19** Numerical velocity distributions for the unsteady boundary conditions (see Fig. II.18).

The results of the numerical simulations are promising. Of course, the numerics is still in progress but we expect to obtain the correlation of the results between the two numerical codes up to the end of the 3<sup>rd</sup> semester of the project.

The focus of the work for the next stage of the project is to perform simulations of the air flow in the presence of mucus and to validate the numerical results with the experiments.

## Conclusions

The main targets of the first year related to the Tasks T5.1 and T5.2 of the project were reached:

- 1) Reconstruction of the test geometry from the CT scan (procedure, geometry, physical test body),
- 2) Rheological characterization of the synthetic mucus sample,
- 3) Design and qualitative testing of the experimental setup,
- 4) Numerical simulations of the air flow in trachea bifurcation using two codes: commercial Ansys Fluent and original code Moebius developed by our partner MedLea.

There are two unfulfillments of the first year, mainly generated by the pandemic situation:

- a. The cooperation with MedLea partner didn't reach yet the optimum. We re-scheduled the working visit of two PhDs from my group at MedLea in the first semester of the next year (hoping that access conditions in the institutions will be back to normal),
- b. The acquisitions of the equipment (optics for visualizations, components, and transducers for the setup) were delayed. Therefore, the experimental investigation of the air flow in the geometry was limited to qualitative visualizations.

**Published papers/Conference participation** (underlined authors are members of the project team)**Journals WOS**

1. Patrascu C., Balan C. (2021) *Planar liquid sheets surrounded by another immiscible liquid at low capillary Reynolds numbers*, Physics of Fluids 33(11), 112103, doi.org/10.1063/5.0069023 (IF 3.521).

**Proceedings WOS (conference papers) – open access**

1. Tanase N.O., Enache A., Broboana D., Balan C. (2021) Experimental and Numerical Studies of the Free Surface Flow over the Patterned Weir, 12th Int. Symp. Adv. Topics in Electrical Eng. (ATEE), Bucharest March 25-27, WOS:000676164800135, doi/10.1109/ATEE52255.2021.9425294.
2. Chiriac E., Bran A.M., Voitincu C., Balan C. (2021) *Experimental Validation of VOF Method in Microchannel Flows*, 12th Int. Symp. Adv. Topics in Electrical Eng. (ATEE), Bucharest March 25-27, WOS: 000676164800041, doi/10.1109/ATEE52255.2021.9425121
3. Botta D., Magos I., Balan C. (2021) *Influence of Viscosity on Radial Diffusion of Fluids in Paper Substrates*, 12th Int. Symp. Adv. Topics in Electrical Eng. (ATEE), Bucharest March 25-27, WOS: 000676164800096, doi/10.1109/ATEE52255.2021.9425224,
4. Magos I., Balan C. (2021) *Contact Angles on Spherical Hydrophilic Surfaces*, 12th Int. Symp. Adv. Topics in Electrical Eng. (ATEE), Bucharest March 25-27, WOS: 000676164800125, doi/10.1109/ATEE52255.2021.9425277.

**registration WOS in progress**

5. Tanase N.O., Broboana D., Balan C. (2021) *Stability of the Lid-Cavity Flow at Low Reynolds Numbers*, 10th Int. Conf. Energy Environment (CIEM), Bucharest Oct. 14-15.
6. Chiriac E., Avram M., Balan C. (2021) *Transition from threads to droplets in a microchannel with liquids with no viscosity contrast*, 10th Int. Conf. Energy Environment (CIEM), Bucharest Oct. 14-15.

**Under review**

Broboana D., Bratu A-M., Magos I., Patrascu C., Balan C. (2021) *Kinematics of the viscous filament during the droplet breakup in air*, submitted for publication in Scientific Reports Nature (open access, IF 5.133); Research Square //doi.org/10.21203/rs.3.rs-955518/v1

Financial

**CHIST-ERA Call**  
**Financial Plan of Project Partner 5<sup>1</sup>**

Principal Investigator	Polytechnic university of bucharest
Institution	Prof. Corneliu Balan
Country	Romania
Funding Organisation	UEFISCDI

Type	Item Description	Year 1		Year 2		Year 3		Year 4		Total	
		Total Costs	Requested	Total Costs	Requested	Total Costs	Requested	Total Costs	Requested	Total Costs	Requested
Personnel <sup>2</sup>	PI(3,6PM), 1PHF (18PM)	2,500.00	2,500.00	26,192.49	26,192.49	14,500.00	14,500.00	1,757.52	1,757.52	44,950.01	44,950.01
Consumables		0.00	0.00	5,000.00	5,000.00	3,000.00	3,000.00	1,000.00	1,000.00	9,000.00	9,000.00
Equipment		0.00	0.00	20,000.00	20,000.00	7,000.00	7,000.00	0.00	0.00	27,000.00	27,000.00
Travel		0.00	0.00	5,000.00	5,000.00	10,000.00	10,000.00	6,000.00	6,000.00	21,000.00	21,000.00
Commissions <sup>3</sup>										0.00	0.00
Other										0.00	0.00
Overheads		500.00	500.00	7,238.51	7,238.51	5,500.00	5,500.00	1,751.48	1,751.48	14,989.99	14,989.99
<b>Total</b>		<b>3,000.00</b>	<b>3,000.00</b>	<b>63,431.00</b>	<b>63,431.00</b>	<b>40,000.00</b>	<b>40,000.00</b>	<b>10,509.00</b>	<b>10,509.00</b>	<b>116,940.00</b>	<b>116,940.00</b>

<sup>1</sup> Some costs may be not eligible in all countries; we recommend checking the Call Announcement and the annex, and consulting with the call national/regional contact points  
<sup>2</sup> Provide information on number of person.months (PM), qualification (e.g. post-doc, technician...)  
<sup>3</sup> E.g. subcontracting, provisions, licensing fees

No.	Type	Cost Euro 1 Euro = 4.87 Lei	Cost Lei	Spent budget	Observation
1	Personnel**	26192.49	127557.43	~142265.28 Lei ~29212.58 Euro	+14707.85 Lei (+3020.09 Euro)
2	Consumables	5000.00	24350.00	48516.13 Lei 9962.24 Euro	+24166.13 Lei
3	Equipment	20000.00	97400.00	72835.80 Lei 14956.01 Euro	-24564.2 (Lei)
<b>Logistics</b>	<b>2 + 3</b>	<b>25000</b>	<b>121750.00</b>	<b>121351.93 Lei 24918.27 Euro</b>	<b>-398.07 Lei (-81.73 Euro)</b>
4	Travel*	5000.00	24350.00	3540.22 Lei 726.95 Euro	-20809.78 Lei (-4273.05 Euro)
5	Overheads**	7238.51	35251.54	~41751.54 Lei ~8573.21 Euro	+6500 Lei (+1334.70 Euro)
6	<b>Total</b>	<b>63431.00</b>	<b>308908.97</b>	<b>308908.97</b>	<b>0.0 Lei/Euro</b>

\*The budget was reduced due to the pandemic conditions; the unspent amount of money was shared between the Personal cost and the Overheads.

\*\* Amount subject to small changes (below 5%)